Influence of Ultrasound on Crystal Growth from Solution and Related Flow Visualization

ARTICLE *in* CRYSTAL GROWTH & DESIGN · SEPTEMBER 2006

Impact Factor: 4.89 · DOI: 10.1021/cg0499313

3 AUTHORS, INCLUDING:

Gennadiy Kozhemyakin
East Ukraine Volodymyr Dahl National Unive…
60 PUBLICATIONS **173** CITATIONS
SEE PROFILE

Yuko Inatomi
Japan Aerospace Exploration Agency
84 PUBLICATIONS **345** CITATIONS
SEE PROFILE

CRYSTAL GROWTH & DESIGN
2006
VOL. 6, NO. 10
2412−2416

Influence of Ultrasound on Crystal Growth from Solution and Related Flow Visualization

G. N. Kozhemyakin,*,† L. V. Zolkina,† and Y. Inatomi‡

Laboratory of Crystal Growth, Department of Applied Materials, The V.Dal Eastern Ukrainian National University, Block Molodezhniy 20 A, Lugansk 91034, Ukraine, and The Institute of Space and Astronautical Science, 3-1-1 Yoshinodai, Sagamihara, Kanagawa 229, Japan

Received February 17, 2004; Revised Manuscript Received June 17, 2006

ABSTRACT: The influence of 3 MHz ultrasound on the growth of GaAs layers by liquid-phase epitaxy was investigated. Ultrasound caused morphological changes in the solid−liquid interface. Distilled water and glycerin were used as model fluids to visualize the flow and ultrasonic standing waves by the light-cut method. Ultrasound at a frequency of 1.0 MHz significantly affected the convection because of the appearance of standing waves.

1. Introduction

In situ observation based on near-infrared microscopy is a unique method for studying the formation, migration, and coalescence of macrosteps on the solid−liquid (S/L) interface during the growth of semiconductor crystals by liquid-phase epitaxy (LPE).[1−5] A number of morphological changes were observed on the S/L interface by this method during solution growth with static and rotating magnetic fields.[6−8] The principal feature of magnetic fields is their effect on convection in the melt and on kinetic processes at the S/L interface. The application of ultrasound as an external field influencing crystal growth is an alternative approach for similar fundamental investigations.[9−14] An important advantage of ultrasound is its directional effect on convection, e.g., perpendicular to the S/L interface.

Convective phenomena play an important role in LPE growth.[1,15,16] The number of experimental investigations of flow in real LPE growth systems is limited because flow cannot be seen under growth conditions. Therefore, model experiments intended to simulate these conditions can be useful for fundamental investigation of the growth processes in LPE systems. Furthermore, model experiments on the influence of ultrasound on convection have been performed only for crystal growth by the Czochralski method.[17,18] Growth conditions in the Czochralski process significantly differ from those in LPE. For this reason, it is difficult to use convection modeling results for Czochralski growth to interpret experimental epitaxial growth results.

The objective of this work was to study the influence of ultrasound on LPE growth in greater detail. Our investigation consisted of two integrated steps: (i) observation of the morphological changes caused by an ultrasonic field during epitaxial growth, and (ii) use of the light-cut method to determine the effect of ultrasound on convection in a simulated LPE system.

2. Experimental Procedures

2.1. Liquid-Phase Epitaxial Growth. Growth experiments were performed in quartz ampules that had been evacuated to 1×10^{-4} mbar and subsequently sealed by mechanical valves (Figure 1).

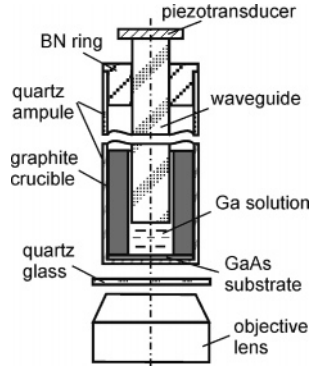

Figure 1. Schematic drawing of setup for liquid-phase epitaxial growth with ultrasonic waves.

Epoxy cement was applied between the quartz ampule wall, fused silica waveguide, and BN ring to maintain the vacuum. The bottom of the ampule was polished to optical flatness. The ampule contained a graphite crucible with a 4 mm inner diameter, 8 mm outer diameter, and 26 mm height. The graphite crucible held 0.8 g of Ga solution and an 8 mm diameter GaAs substrate fastened by Graphi-Bond 669 glue to the bottom. The substrate was 300 μm thick and had an orientation of (111)B. Ultrasonic waves at a frequency of 3 MHz, from 7.4×10^{-4} to 0.036 W/cm^2 acoustic intensity, were introduced into the Ga solution by a piezotransducer through a fused silica waveguide with a 3.7 mm diameter and 265 mm length. The distance between the GaAs substrate and the lower end of the waveguide was 8 mm. The growth was performed with and without ultrasound by the linear cooling method with a starting growth temperature of 816 K and a cooling rate of 0.25 K/min with a temperature gradient of $dT/dx = 8$ K/cm in the solution. The temperature gradient was measured using ceramic-coated K-type (chromel−alumel) thermocouples placed in the crucible.

The morphology of the faceted region of the S/L interface was observed using near-infrared (NIR) microscopy.[6] The imaging beam reflected from the S/L interface was received by a CCD camera without its optical filter in order to improve infrared transparency. The image was recorded on a videotape recorder through an image processing system.

Twelve grown samples were etched with 20% HCl for 5−10 min, and the surface of the growth layer was analyzed by Nomarski interference contrast microscopy. The shape of the interface was studied in a few samples by cutting them parallel to the growth direction and observing them using an Olympus-OLS1000 laser microscope.

2.2. Physical Model of LPE Growth. Convective phenomena in an ultrasonic field for the present LPE growth process were modeled using the light-cut method with transparent fluids. The dimensions of the prototype experimental setup were enlarged by a factor of 5 from the original graphite crucible size (Figure 2).

* To whom correspondence should be addressed. E-mail: kozhem@cci.lg.ua.
† Ukranian National University.
‡ The Institute of Space and Astronautical Science.

10.1021/cg0499313 CCC: $33.50
Published on Web 09/16/2006

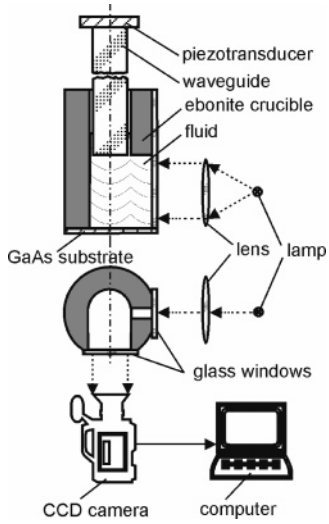

Figure 2. Schematic representation of light-cut technique for flow visualization in model fluids with ultrasonic waves.

Either distilled water or glycerin was used as model fluids. The liquid was contained in an ebonite crucible with a 21 mm inner diameter, 40 mm outer diameter, and 90 mm height, with two glass windows for light beam and flow observation. Ultrasonic waves at a frequency of 1 MHz were introduced into the liquid from a piezotransducer through a fused silica waveguide with a 20 mm diameter and 100 mm length. The direction of the ultrasonic waves was parallel to the crucible axis. A 1 mm thick polymer heater was used to heat the GaAs substrate. The temperature in the liquid under the waveguide and above the substrate was measured using two ceramic-coated K-type thermocouples.

Tracer particles of a textolite with a density of 1270 kg/m^3 were suspended in the liquid, and a light-cut technique was used for flow visualization. These particles were 50 μm diameter spheres. Particle motion was observed using a vertical light cut. A CCD camera was installed such that the flow in the model fluid could be viewed and recorded on video. Flow velocities were calculated by determining the position coordinates of tracer particles in consecutive video frames.

The influence of ultrasound on particle motion was observed under the waveguide using digital image processing software Ulead VideoStudio 4. Several parameters were varied independently in the simulation experiments: temperature difference ΔT, fluid depth h, intensity I, and ultrasound frequency f of the piezotransducer.

3. Results and Discussion

3.1. Growth in an Ultrasonic Field. It is known that the shape of the S/L interface is a very important parameter that influences the homogeneity in crystals grown by the Czochralski method in an ultrasonic field.[12,14] Therefore, we optimized the temperature conditions in the solution to create a flat S/L interface. Figure 3 shows curved and flat S/L interfaces in the presence of 3 MHz ultrasonic waves.

The first crystallization centers and steps were observed on the S/L interface upon decreasing the Ga solution temperature by 3−5 K. Subsequently, a great number of macrosteps emerged on the curved interface, but only one on the flat interface. The growth layers had different morphologies with and without ultrasound. On layers grown with a curved S/L interface, we observed a few macrosteps even for growth in the ultrasound field. The size of these macrosteps decreased during the growth (Figures 3d and 4a). On the other hand, one macrostep was observed after LPE growth on a flat S/L interface in an ultrasonic field at acoustic intensities from 7.4×10^{-4} to 0.036 W/cm^2 (Figures 3d$_1$, 3e$_1$, and 4b).

The macrostep morphology changed within a few minutes of switching on the ultrasound. One macrostep was observed

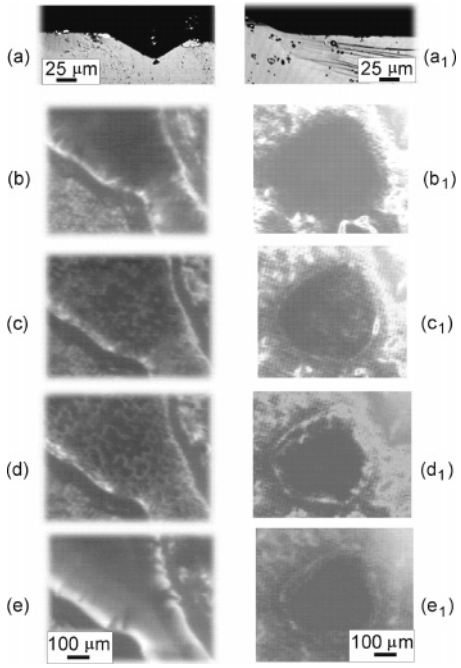

Figure 3. Influence of ultrasound on crystal growth with curved (a−e) and flat (a$_1$−e$_1$) solid−liquid interfaces.

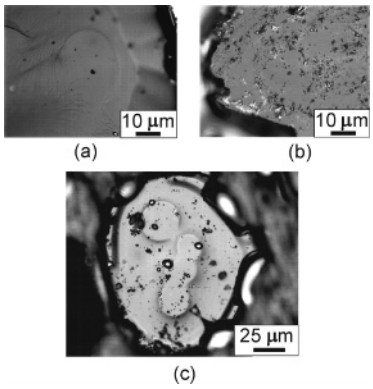

Figure 4. Shape of GaAs epilayers grown in the presence of ultrasonic waves from a Ga solution: (a) curved S/L interface; (b) flat S/L interface; (c) flat S/L interface after switching off the ultrasound.

in such experiments. However, the macrostep growth converted to ordinary growth with a few macrosteps within 2 min of switching off the ultrasound. For example, a growth layer with one macrostep transformed into a layer with four macrosteps on this otherwise atomically smooth plane after switching off the ultrasound (Figure 4c). Switching on the ultrasound promoted the growth of these four steps, resulting in a merge into one atomically smooth macrostep.

3.2. Differences between the Simulation Model and the LPE Setup. An ebonite crucible was used in our simulations. The real growth crucible had a thermally insulated lateral wall. The fluid flow was viewed without distortion in the plane of the image because of the two flat glass windows on the crucible. As noted above, distilled water and glycerin were used as model fluids. These fluids and molten gallium solution have similar values of the Rayleigh number (Ra) but different values of the Prandtl number (Pr). The relevant physical properties and dimensionless numbers for molten Ga, distilled water, and glycerin are given in Table 1.

Various flow phenomena were demonstrated in AVI video format and could be viewed on any PC but not played in real

Table 1. Properties and Non-Dimensional Numbers of Fluids

	molten Ga	distilled water	glycerin
fluid depth h (m)	0.8×10^{-2}	$(2-4) \times 10^{-2}$	$(2-4) \times 10^{-2}$
ΔT (K)	6.4	0.5−4	3−33
ρ (kg/m^3)	5600	1000	1260
kinematic viscosity ν (m^2/s)	0.07×10^{-6}	1×10^{-6}	1174.6×10^{-6}
thermal conductivity λ (W m^{-1} K^{-1})	29.3	0.644	0.288
heat capacity C_p (J kg^{-1} K^{-1})	400	4183.3	2358
thermal diffusivity, $a = \lambda/(C_p\rho)$ (m^2/s)	1.3×10^{-5}	0.0153×10^{-5}	9.7×10^{-8}
thermal coefficient of volume expansion, α (K^{-1})	0.1×10^{-3}	0.2×10^{-3}	0.505×10^{-3}
Rayleigh number, Ra $= g\alpha\Delta T h^3/a\nu$	0.35×10^4	$(5-328) \times 10^4$	$(0.1-9.3) \times 10^4$
Prandtl number, Pr $= \nu/a$	5.4×10^{-3}	6.54	1.2×10^4

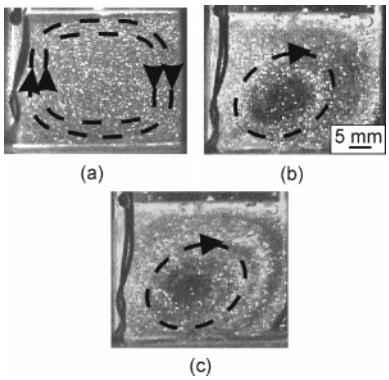

Figure 5. Flow patterns with a fluid depth h of 20 mm in (a) water at $\Delta T = 2$ K; (b) glycerin at $\Delta T = 13$ K; and (c) glycerin at $\Delta T = 17$ K.

time. Particle velocities were measured using a monitor and a time label of the CCD camera.

3.3. Convection Pattern without Ultrasound. The first flow pattern could be observed in distilled water at $h = 20$ mm and $\Delta T > 0.1$ K a few seconds after switching on the heater. Figure 5a shows the characteristic features of the flow for $\Delta T = 2$ K ($dT/dx = 1$ K/cm). The flow was symmetric and in a clockwise direction around the center of the fluid volume. The maximum flow velocity was 0.6 mm/s under the surface of the waveguide, below the substrate, and in the vertical flow near the wall of the crucible. The flow pattern velocity increased with increasing temperature difference.

For a given system, in experiments using glycerin with $h = 20$ mm, the flow structure had one vortex, which appeared only after 20 min from switching on the heater with a ΔT of more than 10 K and gradient $dT/dx = 5$ K/cm. The center of the vortex was located at the center of the glycerin volume (Figure 5b). As shown in Figure 5c, the flow rotated clockwise in this vortex and had elliptic streamlines with a maximum flow velocity of 0.3 mm/s at $\Delta T = 16.5$ K ($dT/dx = 8.25$ K/cm). The flow velocity decreased with increasing glycerin depth.

Buoyancy-induced flow in a fluid is expected to increased with an increase in fluid depth h, because the Rayleigh number is proportional to the fluid depth h cubed. In water with $h = 40$ mm and $\Delta T < 2$ K ($dT/dx < 0.5$ K/cm), we observed flow features similar to those with $h = 20$ mm (Figure 6a). The maximum flow velocity was equal to 0.3 mm/s in these flow patterns. For $h = 40$ mm and $\Delta T = 4$ K ($dT/dx = 1$ K/cm), there were two counter-rotating vortices symmetrical to the axis of the crucible (Figure 6b). The maximum flow velocity had increased to 0.6 mm/s.

In glycerin, for the same depth and $\Delta T > 6$ K ($dT/dx > 1.5$ K/cm), there were two round vortices of equal size but rotating in opposite directions (Figure 6c). The maximum velocity was 0.5 mm/s in the flow moving downward along the crucible wall, over the substrate, and upward from the substrate near the lower vortex.

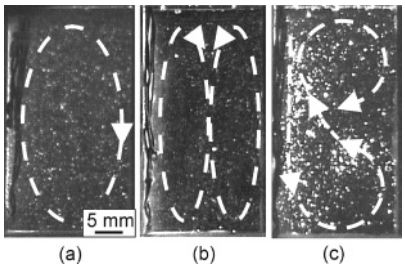

Figure 6. Flow patterns with fluid depth $h = 40$ mm in (a) water at $\Delta T < 2$ K; (b) water at $\Delta T = 4$ K; and (c) glycerin at $\Delta T > 6$ K.

The different flow patterns in water and glycerin may be explained using dimensionless numbers. The lower flow velocity for glycerin compared to water is expected because the Rayleigh number of glycerin is smaller, primarily because of glycerin's much higher kinematic viscosity. The flow structure in molten Ga is likely to be closer to the flow in glycerin, because the difference in their Rayleigh numbers is smaller.

3.4. Influence of Ultrasound on Convection in the Fluids. The morphology of the faceted region of the S/L interface is affected by the flow patterns in the solution during liquid-phase epitaxy growth.[1,15,16] The fluid can become stagnant only under the strong influence of an ultrasonic field in which the ultrasonic waves are transmitted from a piezotransducer through a waveguide to the entire fluid volume. The low intensity and high frequency of ultrasound in our experiments gave rise to standing waves in the fluids. This phenomenon can be explained by the waveguide having a flat surface parallel to the flat surface of the substrate and the fluid depth being greater than the ultrasound wavelength.

For a given system, the influence of a standing wave on a suspended particle can be correlated to force F_r acting on an incompressible particle in a running wave. This force is[19]

$$F_r = 2/9\pi R^2 (kR)^4 \rho v^2 (a_1^2 + a_1 a_2 + 3/4 a_2^2) \qquad (1)$$

where R is the radius of the particle, k is the wavenumber, $\rho$is the density of the fluid, v is the particle velocity in the ultrasonic wave, $a_1 = 1 - \rho\xi^2/\rho_p\xi_p^2$, $a_2 = 2(\rho_p - \rho/2\rho_p + \rho)$, ρ_p is density of the particle, and ξ and ξ_p are the sound velocities in the fluid and in the particle, respectively, in the direction of wave propagation.

When ultrasound waves encounter a flat barrier, e.g., the S/L interface, they form ultrasonic standing waves in the liquid. The force F_s acting on a particle in an ultrasonic standing wave can then be written as[19]

$$F_s = \pi R^2 (kR) \rho v^2 \left[\frac{\rho_p + \frac{2}{3}(\rho_p - \rho)}{2\rho_p + \rho} - \frac{\rho\xi^2}{3\rho_p \xi_p^2} \right] \qquad (2)$$

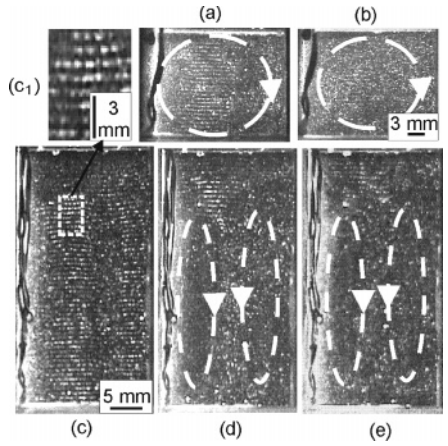

Figure 7. Standing waves and flow patterns in water at different depths and temperature differences: (a) $h = 20$ mm, $\Delta T = 1.5$ K ($dT/dx = 0.75$ K/cm); (b) $h = 20$ mm, $\Delta T = 2.3$ K ($dT/dx = 1.15$ K/cm); (c) $h = 40$ mm, $\Delta T = 0.2$ K ($dT/dx = 0.05$ K/cm); (c_1) distribution of the particles in standing waves; (d) $h = 40$ mm, $\Delta T = 2$ K ($dT/dx = 0.5$ K/cm); (e) $h = 40$ mm, $\Delta T = 3$ K ($dT/dx = 0.75$ K/cm).

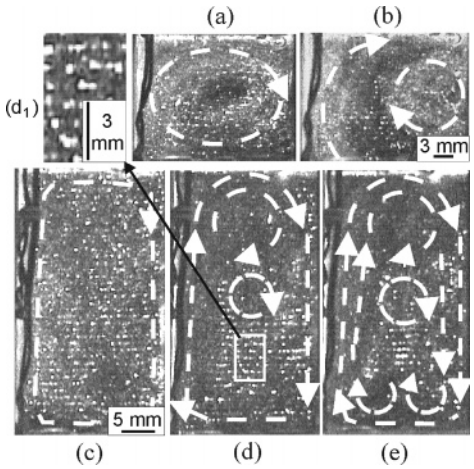

Figure 8. Standing waves and flow patterns in glycerin at different depth and temperature gradients: (a) $h = 20$ mm, $\Delta T = 3$ K ($dT/dx = 1.5$ K/cm); (b) $h = 20$ mm, $\Delta T = 4$ K ($dT/dx = 2$ K/cm); (c) $h = 40$ mm, $\Delta T = 8$ K ($dT/dx = 2$ K/cm); (d) $h = 40$ mm, $\Delta T = 20$ K ($dT/dx = 5$ K/cm); (d_1) distribution of particles in standing waves; (e) $h = 40$ mm, $\Delta T = 33$ K ($dT/dx = 8.25$ K/cm).

These forces have an effect on any incompressible particles with $R \ll \lambda$. The wavelength of ultrasonic waves was $\lambda > 1$ mm in the fluids and melts in all our experiments. Additionally, the force F_s was larger than the calculated buoyancy force by a factor of more than 200 in our experiments. Because the radius of atoms or molecules in the solution is less than $R \approx 1$ nm, $F_s > F_r$ by 4 orders of magnitude. Therefore, ultrasound standing waves can reduce buoyant convection because of particle oscillation in the wave antinodes.

Experimentally, introduction of ultrasound into a transparent fluid generates standing waves under certain conditions. As seen in Figure 7a, thin white layers were oriented parallel to the substrate surface in water with $h = 20$ mm at $\Delta T = 1.5$ K ($dT/dx = 0.75$ K/cm). These layers consisted of oscillating particles in standing wave antinodes. The distance between adjacent layers was 0.77 mm, which conforms to half the ultrasound wavelength in distilled water at a frequency of 1 MHz. The formation time of standing waves was 2−4 s after switching on the ultrasound. The disappearance of the standing waves was not instantaneous, but in water required 3−6 s after switching off the ultrasound. Standing waves stopped the motion of the flow patterns in the central region of the water where the flow velocity was low. The size of the standing wave region diminished with increasing temperature difference $\Delta T > 2$ K ($dT/dx > 1$ K/cm) (Figure 7b).

Figure 7c−e shows the effect of the temperature difference ΔT on the flow pattern and standing waves in water with $h = 40$ mm. When the temperature difference ΔT was increased from 0.2 to 3 K, the flow became more vigorous and standing waves deformed. The convection was completely damped by standing waves at $\Delta T > 3$ K ($dT/dx > 0.75$ K/cm). Here, the Rayleigh number was 8 times higher at $h = 40$ mm than at $h = 20$ mm for the same temperature gradient.

Ultrasonic standing waves also appeared in glycerin 2−4 s after switching on the ultrasound and had a 6−8 s renewal time of the flow after switching off the ultrasound. The distance between the layers with maximum concentrations of particles was 1 mm (Figure 8). This value is close to half the wavelength of the ultrasound wave in glycerin (0.92 mm at a frequency of 1 MHz and 30 °C).

Figure 8 shows the influence of convection on the formation of standing waves in glycerin. The increase in depth from $h = 20$ mm to $h = 40$ mm and an increasing temperature difference ΔT from 3 to 33 K destroyed the ultrasonic standing waves because of the enhanced convective heat flow extending from the periphery to the center of the glycerin volume. For these conditions, the Rayleigh number Ra increased from 0.1×10^4 to 0.93×10^5. However, even for $h = 40$ mm and a temperature gradient $dT/dx = 8.25$ K/cm, these standing waves could be observed in the central region of the crucible. In addition, the ultrasound decreased the maximum particle velocity by about half, from 0.5 mm/s down to 0.23 mm/s.

4. Conclusions

The influence of an ultrasonic field on the morphology of the interface during liquid-phase epitaxial growth of GaAs was shown experimentally. The introduction of 3 MHz ultrasonic waves in a Ga solution promoted the conditions for LPE growth with a flat S/L interface. Ultrasonic waves changed the macrostep morphology within a few minutes of switching on the ultrasound. The appearance of one macrostep on a flat S/L interface converted to several macrosteps within 2 min of switching off the ultrasound.

Distilled water and glycerin, which have Rayleigh numbers similar to that of molten Ga, were used as model fluids. Using the light-cut method and digital image processing, we developed a method for observing the convection stability under the presence of ultrasonic waves. The ebonite crucible was five times larger than the graphite crucible used for LPE growth. The flow velocity in distilled water and glycerin at different fluid depths and temperature gradients was measured experimentally using suspended tracer particles. The maximum flow velocity for $h = 40$ mm was 0.6 mm/s with $dT/dx = 1$ K/cm and 0.5 mm/s with $dT/dx = 8.25$ K/cm) for water and glycerin, respectively. The increase in the fluid depth and temperature gradient created a few vortices in the fluids.

We showed that ultrasound at a high frequency can be used for reduction of convection in solution crystal growth by liquid-phase epitaxy. The strong reduction of flow motion is associated with the formation of standing waves between the S/L interface and the waveguide. The above phenomenon is theoretically explained by the force F_s acting on a particle with $R \ll \lambda$ in ultrasound standing wave being 4 orders of magnitude higher than the force F_r acting on a particle in running wave. This

force F_s can be greater than the buoyancy force acting on atoms or molecules in flow patterns under certain growth conditions and temperature gradients when the Rayleigh number Ra $< 1 \times 10^5$.

The convincing evidence for the presence of standing waves in our model experiments was the distribution of buoyant particles, where the maximum concentration was at standing wave antinodes. The onset time for standing waves in the model fluids was 2−4 s in our experiments. However, the disappearance time of standing waves was different in water and glycerin, 3−6 and 6−8 s, respectively.

Increasing the liquid depth from $h = 20$ mm to $h = 40$ mm and the temperature difference ΔT from 3 to 33 K destroyed ultrasonic standing waves because of the enhanced convective heat flow extending from the periphery to the center of the glycerin volume; this agrees with the increase in the Rayleigh number from 1.04×10^3 to 0.93×10^5. Ultrasound decreased the maximum particle velocity in the flow patterns to half under given conditions of the experiment.

The results of these experiments indicate a promising application for ultrasound in liquid epitaxial growth.

Acknowledgment. The authors would like to thank Professor K. Kuribayashi for invitation and technical support. The opportunity to grow and observe the epitaxial layers at the Institute of Space and Astronautical Science is greatly appreciated.

Supporting Information Available: Short video clips of the flow patterns in glycerin without ultrasound and standing waves and flow patterns in water before and after switching on ultrasound. This material is available free of charge via the Internet at http://pubs.acs.org.

References

(1) Danilewsky, A. N.; Dold, P.; Benz, K. W. *J. Cryst. Growth* **1992**, *121*, 305−314.
(2) Dold, P.; Benz, K. W. *Cryst. Res. Technol.* **1995**, *30*, 1135−1144.
(3) Dold, P.; Benz, K. W. *Cryst. Res. Technol.* **1997**, *32*, 51−60.
(4) Inatomi, Y.; Kuribayashi, K. *J. Cryst. Growth* **1993**, *128*, 557−561.
(5) Inatomi, Y.; Dold, P.; Danilewski, A. N.; Benz, K. W. *Cryst. Res. Technol.* **1997**, *32*, 759−768.
(6) Inatomi, Y.; Aoki, S.; Kuribayashi, K.; Sawada, Y. *Cryst. Res. Technol.* **1998**, *33*, 857−866.
(7) Inatomi, Y.; Kuribayashi, K. *J. Cryst. Growth* **2002**, *241*, 395−403.
(8) Kaiser, Th.; Benz, K. W. *Phys. Fluids* **1998**, *10*, 1104−1110.
(9) Hayakawa, Y.; Kumagawa, M. *Cryst. Res. Technol.* **1985**, *20*, 3−10.
(10) Hayakawa, Y.; Kumagawa, M. *Jpn. J. Appl. Phys.* **1988**, *27*, 47−49.
(11) Kozhemyakin, G. N.; Kosushkin, V. G.; Kurochkin, S. Y. *J. Cryst. Growth* **1992**, *121*, 240−242.
(12) Kozhemyakin, G. N.; Kolodyazhnaya, L. G. *J. Cryst. Growth* **1995**, *147*, 200−206.
(13) Kozhemyakin, G. N. *J. Cryst. Growth* **1995**, *149*, 266−268.
(14) Kozhemyakin, G. N. *Ultrasonics* **1998**, *35*, 599−604.
(15) Fisher, B.; Friedrich, J.; Weimann, H.; Muller, G. *J. Cryst. Growth* **1999**, *198/199*, 170−175.
(16) Inatomi, Y.; Kuribayashi, K. *J. Cryst. Growth* **2002**, *241*, 395−403.
(17) Hayakawa, Y.; Sone, Y.; Ishino, F.; Kumagawa, M. *Jpn J. Appl. Phys.* **1983**, *22* (No.1), 206.
(18) Kozhemyakin, G. N. *J. Cryst. Growth* **2003**, *257*, 237−244.
(19) Agranat, B. A.; Dubrovin, M. N.; Havskiy N. N.; Eskin, G. I. In *Basics of Physics and Techniques of Ultrasound*; High School: Moscow, 1987; pp 90−93 (in Russian).

CG0499313